Alexandria Engineering Journal (2022) 61, 10045–10053

HOSTED BY

Alexandria University

Alexandria Engineering Journal

www.elsevier.com/locate/aej
www.sciencedirect.com

Heat transfers thermodynamic activity of a second-grade ternary nanofluid flow over a vertical plate with Atangana-Baleanu time-fractional integral

Nehad Ali Shah [a], Abderrahim Wakif [b], Essam R. El-Zahar [c,d], Thirupathi Thumma [e], Se-Jin Yook [f,*]

[a] *Department of Mechanical Engineering, Sejong University, Seoul 05006, Korea*
[b] *Hassan II University, Faculty of Sciences Aïn Chock, Laboratory of Mechanics, Casablanca, Morocco*
[c] *Department of Mathematics, College of Science and Humanities in Al-Kharj, Prince Sattam Bin Abdulaziz University, P.O. Box 83, Al-Kharj 11942, Saudi Arabia*
[d] *Department of Basic Engineering Science, Faculty of Engineering, Menoufia University, Shebin El-Kom 32511, Egypt*
[e] *Department of Mathematics, B V Raju Institute of Technology, Narsapur, Medak 502313, Telangana State, India*
[f] *School of Mechanical Engineering, Hanyang University, 222 Wangsimni-ro, Seongdong-gu, Seoul 04763, Republic of Korea*

Received 20 December 2021; revised 8 March 2022; accepted 19 March 2022

KEYWORDS

Heat transfers;
Second-grade ternary nanofluid;
Atangana-Baleanu time-fractional integral;
Generalized Fourier's law;
Laplace transform

Abstract The impact of the Atangana-Baleanu (AB) time-fractional integral on second-grade fluid with ternary nanoparticle suspension across an infinite vertical plate was studied in this paper. By generalized Fourier's law, the generalized fractional constitutive equation for the thermal flux explains a thermal process with memory. Closed-form solutions are calculated using Laplace transform and represented using Lorenzo and Hartley G–functions and integral forms. The numerical effects of physical and fractional parameters are presented.

1. Introduction

Fractional calculus (FC) is a new discipline in science and engineering that deals with mathematical modeling of real-world issues. The restrictions of integer ordered differential calculus are addressed by fractional ordered derivatives. Many scientists and researchers are using FC to apply real-world complex dynamics in fields such as physics, biology, electrochemistry, mechatronics, bioengineering, signal and image processing, environmental science, and economics because FC understands fading memory effects and boundary behavior that arise in physical and biological systems [1,2]. Many current models of physical processes have been effectively modified using fractional calculus. Abel used fractional calculus to solve an integral equation that emerges in the formulation of the

* Corresponding author.
E-mail addresses: nehadali199@yahoo.com, nehadali199@sejong.ac.kr (N.A. Shah), abderrahim.wakif-etu@etu.univh2c.ma (A. Wakif), er.elzahar@psau.edu.sa (E.R. El-Zahar), ysjnuri@hanyang.ac.kr (S.-J. Yook).

Peer review under responsibility of Faculty of Engineering, Alexandria University.

https://doi.org/10.1016/j.aej.2022.03.048

tautochrone issue, which was the first use of fractional derivatives. The whole theory of fractional derivatives and integrals can be said to have been established in the second half of the nineteenth century. When utilizing fractional derivatives to describe viscoelastic materials, Caputo and Mainardi [3,4] and Caputo [5] found good agreement with experimental data and established a link between fractional derivatives and the theory of linear viscoelasticity. A comprehensive list of the latest applications of ordered fractional calculus was found in [6–9].

The fractional derivatives are adopted to represent the effects of a long time - memory, which is essential while modeling fluid flows depends on the flow history. The time-fractional derivative attracted numerous researchers due to their potential applications in epidemiology modeling, quantum mechanics, tuberculosis (TB) disease modeling, applied physics and chemistry, viscoelasticity, Ebola treatment, Cancer therapy, and modeling of Chaotic systems Biofluids. The thermal conductivity of conventional fluids plays a vital role in governing the heat transfer rate between medium and surface. In comparison to the base fluids with low thermal conductivity, nanofluids have more excellent thermal properties. Still, investigators recently established a novel fluid, namely, Hybrid Nanofluid (HNF), in which two types of nanoparticles are dispersed in a base fluid. These HNFs have many prospective applications such as microelectronics, microfluidics, medical, transportation, acoustics, defense, and chemical catalytic reactors [10–13].

Two forms of fluids have changed the dynamics of today's world: Newtonian and non-Newtonian fluids. Researchers first concentrated on Newtonian fluids, but the relevance of non-Newtonian fluids is expanding due to the complexity and variety of multiple fluid-dependent procedures. Non-Newtonian fluids are useful in a wide range of applications, including economic, industrial, physiological, mechanical, physical, medicinal, and technological. As a result, for a better understanding of such occurrences, a narrative of non-Newtonian fluids is required. It's possible to do so by contrasting Newtonian and non-Newtonian fluid properties. The difference between Newtonian and non-Newtonian fluids is that Newtonian fluids have a linear relationship between shear and strain rates, but non-Newtonian fluids do not. As a result of this connection, non-Newtonian fluids have a variety of properties and are classified as shear thinning, shear thickening, dilatant, and thixotropic fluids. Rheologists revealed that different fluid models, such as second-grade fluid, which describes shear thinning and thickening features, and Newtonian fluid, behave differently in different scenarios. Because of its dynamical properties, second-grade fluid is well-known and valuable among researchers [14–19].

The thorough literature introduced above endorses. To the best of the author's acquaintance, the diminutive consideration is paid towards assessing buoyancy and heat source/sink effects on ternary second grade nanofluid incompressible transient flow above the sinusoidal oscillating upright surface. Therefore, the principal attention of the present investigation is heat transfer analysis and thermodynamic activity of a second-grade ternary nanofluid flow over an oscillating vertical plate with Atangana-Baleanu time-fractional integral. The resulting flow governing equations are solved utilizing a widely accepted Laplace Transform Technique (LTT). The computational results obtained through MATHCAD software are validated in the limiting cases of the fractional integral. The illustrative images of boundary layer profiles for velocity and thermal flow are illustrated. The friction factor and rate of heat transfer values are tabularized and explained.

2. Mathematical formulation and solution of the problem

Consider an incompressible second-grade ternary nanofluid lying in a plane over an infinite rigid flat plate. The $x-$axis is parallel to the plate and $y-$axis is taken normal to the plate. Initially, the fluid and the plate are at rest. After a time$t = 0^+$, the plate begins to moving in its plane with velocity$\vartheta_0 f(t)$, where ϑ_0 is the constant velocity and $f(\cdot)$ is Laplace transformable function with$f(0) = 0$. At the same time, the plate temperature is raised/lower to χ'_w which is maintained constant. We assume that the velocity and temperature are the functions of y and t only. For such a flow, the constrain of incompressibility is identically satisfied. Under the assumption of no pressure gradient in flow direction and Boussinesq's approximation, the unsteady flow governed by the following set of partial differential equations [20,21].

Equation of momentum.

$$\rho_{mnf}\frac{\partial \vartheta'(y,t)}{\partial t} = \mu_{mnf}\frac{\partial^2 \vartheta'(y,t)}{\partial y^2} + \alpha_1\frac{\partial^3 \vartheta'(y,t)}{\partial y^2 \partial t} + g(\rho\beta_{\chi'})_{mnf}[\chi'(y,t) - \chi'_\infty];\ y,\ t > 0, \tag{1}$$

Thermal balance equation.

$$(\rho c_p)_{mnf}\frac{\partial \chi'(y,t)}{\partial t} = -\frac{\partial q(y,t)}{\partial y};\ y,\ t > 0, \tag{2}$$

Fourier's law.

$$q(y,t) = -k_{mnf}\frac{\partial \chi'(y,t)}{\partial y}, \tag{3}$$

where

ϑ'- Component of velocity	x& y-Cartesian coordinates.
μ- Dynamic viscosity	ρ - Density
g - Gravitational acceleration	$\beta_{\chi'}$ - Thermal expansion factor
χ' - Temperature	χ'_w - Temperature of the sheet
χ'_∞ - Ambient temperature	k - Thermal conductivity
c_p - Specific heat	Q - Heat source/sink

The thermophysical characteristics that are effective are specified by (see Sundar et al. [22]).ariation.Basel) 2020, d plate,

2.1. Ternary nanofluid

$$\mu_{mnf} = \frac{\mu_f}{(1-(\phi_1+\phi_2+\phi_3))^{2.5}}$$

$$\rho_{mnf} = (1-(\phi_1+\phi_2+\phi_3))\,\rho_f + \phi_1\rho_{S1} + \phi_2\rho_{S2} + \phi_3\rho_{S3}$$

$$(\rho c_p)_{mnf} = (1-(\phi_1+\phi_2+\phi_3))(\rho c_p)_f + \phi_1(\rho c_p)_{S1} + \phi_2(\rho c_p)_{S2} + \phi_3(\rho c_p)_{S3}$$

$$(\rho\beta_{\chi'})_{mnf} = (1-(\phi_1+\phi_2+\phi_3))(\rho\beta_{\chi'})_f + \phi_1(\rho\beta_{\chi'})_{S1} + \phi_2(\rho\beta_{\chi'})_{S2} + \phi_3(\rho\beta_{\chi'})_{S3}$$

$$\frac{k_{mnf}}{k_{bf}} = \frac{\phi_1k_1+\phi_2k_2+\phi_3k_3+2(\phi_1+\phi_2+\phi_3)k_f+2(\phi_1+\phi_2+\phi_3)(\phi_1k_1+\phi_2k_2+\phi_3k_3)-2(\phi_1+\phi_2+\phi_3)^2k_f}{\phi_1k_1+\phi_2k_2+\phi_3k_3+2(\phi_1+\phi_2+\phi_3)k_f-(\phi_1+\phi_2+\phi_3)(\phi_1k_1+\phi_2k_2+\phi_3k_3)+(\phi_1+\phi_2+\phi_3)^2k_f}$$

2.2. Hybrid nanofluid

$$\mu_{hnf} = \frac{1}{\mu_f^{-1}(1-(\phi_1+\phi_2))^{2.5}}$$

$$\rho_{hnf} = (1-(\phi_1+\phi_2))\rho_f + \phi_1\rho_{S1} + \phi_2\rho_{S2}$$

$$(\rho c_p)_{hnf} = (1-(\phi_1+\phi_2))(\rho c_p)_f + \phi_1(\rho c_p)_{S1} + \phi_2(\rho c_p)_{S2}$$

$$(\rho\beta_{\chi'})_{hnf} = (1-(\phi_1+\phi_2))(\rho\beta_{\chi'})_f + \phi_1(\rho\beta_{\chi'})_{S1} + \phi_2(\rho\beta_{\chi'})_{S2}$$

$$\frac{k_{hnf}}{k_{bf}} = \frac{\phi_1k_1+\phi_2k_2+2(\phi_1+\phi_2)k_f+2(\phi_1+\phi_2)(\phi_1k_1+\phi_2k_2)-2(\phi_1+\phi_2)^2k_f}{\phi_1k_1+\phi_2k_2+2(\phi_1+\phi_2)k_f-(\phi_1+\phi_2)(\phi_1k_1+\phi_2k_2)+(\phi_1+\phi_2)^2k_f}$$

2.3. Mano nanofluid

$$\mu_{nf} = \frac{1}{\mu_f^{-1}(1-(\phi_1))^{2.5}}$$

$$\rho_{nf} = (1-(\phi_1))\rho_f + \phi_1\rho_{S1}$$

$$(\rho c_p)_{nf} = (1-(\phi_1))(\rho c_p)_f + \phi_1(\rho c_p)_{S1}$$

$$(\rho\beta_{\chi'})_{nf} = (1-(\phi_1))(\rho\beta_{\chi'})_f + \phi_1(\rho\beta_{\chi'})_{S1}$$

$$\frac{k_{nf}}{k_{bf}} = \frac{\phi_1k_1+2(\phi_1)k_f+2(\phi_1)(\phi_1k_1)-2(\phi_1)^2k_f}{\phi_1k_1+2(\phi_1)k_f-(\phi_1)(\phi_1k_1)+(\phi_1)^2k_f}$$

The expressions mentioned above ϕ_1, ϕ_2 and ϕ_3 denoted the solid volume fractions of Cu, Al_2O_3, and Ag, respectively.

Initial and boundary conditions that are suitable involve:

$$\vartheta'(y,0)=0,\ \ \chi'(y,0)=\chi'_\infty;\ \ y>0, \tag{4}$$

$$\vartheta'(0,t)=\vartheta_0 f(t),\ \ \chi'(0,t)=\chi'_w,\ \ t>0, \tag{5}$$

$$\vartheta'(y,t)\to 0,\ \ \chi'(y,t)\to\chi'_\infty asy\to\infty,\ \ t>0. \tag{6}$$

In Eqs. (1)–(6), add the dimensionless variables mentioned following:

$$\left.\begin{aligned}\Im=\frac{\vartheta_0^2 t}{\nu_{mnf}},\ \Upsilon=\frac{\vartheta_0 y}{\nu_{mnf}},\ \vartheta=\frac{\vartheta'}{\vartheta_0},\ \chi=\frac{\chi'-\chi'_\infty}{\chi'_w-\chi'_\infty}, q^*=\frac{q}{q_0},\ q_0=\frac{k_{mnf}(\chi'_w-\chi'_\infty)\vartheta_0}{\nu_{mnf}},\\ \eta=\frac{\alpha_1\vartheta_0^2}{(\mu\nu)_{mnf}},\ Gr=\frac{g(\nu\beta_{\chi'})_{mnf}(\chi'_w-\chi'_\infty)}{\vartheta_0^3},\ \Pr=\frac{(\mu c_p)_{mnf}}{k_{mnf}},\end{aligned}\right\} \tag{7}$$

we get the non-dimensionless problem by removing the star notations

$$\frac{\partial\vartheta(\Upsilon,\Im)}{\partial\Im}=\frac{\partial^2\vartheta(\Upsilon,\Im)}{\partial\Upsilon^2}+\eta\frac{\partial^3\vartheta(\Upsilon,\Im)}{\partial\Upsilon^2\partial\Im}+Gr\chi(\Upsilon,\Im), \tag{8}$$

$$\frac{\partial\chi(\Upsilon,\Im)}{\partial\Im}=-\frac{1}{\Pr}\frac{\partial q(\Upsilon,\Im)}{\partial\Upsilon}, \tag{9}$$

$$q(\Upsilon,\Im)=-\frac{\partial\chi(\Upsilon,\Im)}{\partial\Upsilon}, \tag{10}$$

$$u(\Upsilon,0)=0,\ \ \chi(\Upsilon,0)=0,\ \ \Upsilon\geqslant 0, \tag{11}$$

$$\vartheta(0,\Im)=f(\Im),\ \ \chi(0,t)=1,\ \ \Im>0, \tag{12}$$

$$\vartheta(\Upsilon,\Im)\to 0,\ \ \chi(\Upsilon,\Im)\to 0\, as\Upsilon\to\infty,\ \ \Im\geqslant 0. \tag{13}$$

where Gr is the Grashof number and Pr is Prandtl number.

In the following part, we'll look at a thermal process with memory, which is described by the generalized fractional thermal flux [23,24].

$$q(\Upsilon,\Im)=-I_\Im^\alpha\left(\frac{\partial\chi(\Upsilon,\Im)}{\partial\Upsilon}\right);\ 0<\alpha<1, \tag{14}$$

where I_t^α is the generalized Atangana-Baleanu fractional integral defined as.

$$\left(I_t^\alpha f\right)(\Im)=(1-\alpha)f(\Im)+\alpha\psi_0(\Im,\alpha)*f(\Im),\ \alpha\in(0,1), \tag{15}$$

with the kernel $\psi_0(t,\alpha)$ which is defined as.

$$\psi_0(\Im,\alpha)=\frac{\Im^{\alpha-1}}{\Gamma(\alpha)} \tag{16}$$

It is observed that $L\{\psi_0(\Im,\alpha)\}=\frac{1}{s^\alpha}$, $\lim_{\alpha\to 0}L\{\psi_0(\Im,\alpha)\}=1=L\{\delta(\Im)\}$, therefore,

$$\lim_{\alpha\to 0}\psi_0(\Im,\alpha)=\delta(\Im) \tag{17}$$

Using the above properties, the fractional integral operator can be defined for$\alpha = 0$.

The fractional integral operator in Eq. (15) has the following properties:

$$\begin{aligned}&\left(I_{\mathfrak{I}}^{0} f\right)(\mathfrak{I}) = \delta(\mathfrak{I}) * f(\mathfrak{I}) = f(\mathfrak{I}),\\ &\left(I_{\mathfrak{I}}^{1} f\right)(\mathfrak{I}) = 1 * f(\mathfrak{I}) = \int_0^{\mathfrak{I}} f(\upsilon) d\upsilon.\end{aligned} \tag{18}$$

3. Solution of the problem

3.1. Temperature distribution

We get the following results by applying the Laplace transform to Eqs. (9), (14), $(12)_2$, $(13)_2$, and utilizing the initial condition in Eq. $(11)_2$:

$$s\,\bar{\chi}(\Upsilon, s) = -\frac{1}{\mathrm{Pr}} \frac{\partial \bar{q}(\Upsilon, s)}{\partial \Upsilon}, \tag{19}$$

$$\bar{q}(\Upsilon, s) = -\left[\frac{(1-\alpha)s^{\alpha} + \alpha}{s^{\alpha}}\right] \frac{\partial \bar{\chi}(\Upsilon, s)}{\partial \Upsilon}, \tag{20}$$

$$\bar{\chi}(0, s) = \frac{1}{s},\ \bar{\chi}(\Upsilon, s) \to 0 \text{ as } \Upsilon \to \infty. \tag{21}$$

The solution of Eqs. (19) and (20) under the conditions of Eq. (21) is represented as

$$\begin{aligned}\bar{\chi}(\Upsilon, s) &= \frac{1}{s} \exp\left(-\Upsilon \sqrt{\frac{\mathrm{Pr} s^{\alpha+1}}{(1-\alpha)s^{\alpha} + \alpha}}\right)\\ &= \frac{1}{s} \exp\left(-\Upsilon \sqrt{\frac{\mathrm{Pr}}{1-\alpha}} \sqrt{\frac{s^{\alpha+1}}{s^{\alpha} + \frac{\alpha}{1-\alpha}}}\right),\end{aligned} \tag{22}$$

For the inverse Laplace transform, Eq. (22) can be written as.

$$\bar{\chi}(\Upsilon, s) = \bar{\chi}_1(s)\bar{\chi}_2(\Upsilon, s), \tag{23}$$

where

$$\begin{aligned}&\bar{\chi}_1(s) = \tfrac{1}{s}\sqrt{\tfrac{s^{\alpha}+b}{s^{\alpha+1}}} = \tfrac{1}{s^{\frac{\alpha+2}{2}}}\sqrt{s^{\alpha}+b} = \tfrac{1}{s^{\frac{\alpha+2}{2}}}\tfrac{s^{\alpha}+b}{\sqrt{s^{\alpha}+b}} == \tfrac{1}{s^{\frac{\alpha-2}{2}}}\tfrac{1}{\sqrt{s^{\alpha}+b}} + \tfrac{b}{\sqrt{s^{\alpha}+b}}\bar{\chi}_2(\Upsilon, s)\\ &= \bar{B}(s)\bar{A}(s) + b\,\bar{A}(s);\quad \bar{B}(s) = \tfrac{1}{s^{\frac{\alpha-2}{2}}},\ \bar{A}(s) = \tfrac{1}{\sqrt{s^{\alpha}+b}},\\ &= \frac{\exp\left(-\frac{a\Upsilon}{\sqrt{w_2(s)}}\right)}{\sqrt{w_2(s)}},\ w_2(s) = \frac{s^{\alpha}+b}{s^{\alpha+1}},\ a = \sqrt{\frac{\mathrm{Pr}}{1-\alpha}} \text{ and } b = \frac{\alpha}{1-\alpha}.\end{aligned}$$

Applying the inverse Laplace transform to Eq. (23), we obtain.

$$\chi(\Upsilon, \mathfrak{I}) = \chi_1(\mathfrak{I}) * \chi_2(\Upsilon, \mathfrak{I}), \tag{24}$$

with $\chi_1(\mathfrak{I}) = B(\mathfrak{I})A(\mathfrak{I}) + bA(\mathfrak{I});\ B(\mathfrak{I}) = \frac{\mathfrak{I}^{\frac{1-\alpha}{2}}}{\Gamma\left(\frac{3-\alpha}{2}\right)},\ A(\mathfrak{I}) = \int_0^{\infty} \frac{1}{\sqrt{\pi u}} \frac{e^{-bu}}{\mathfrak{I}} \Phi(0, -\alpha; -u\mathfrak{I}^{-\alpha}) du,$.

where $\mathfrak{I}^{\beta-1}\Phi(\beta, -\sigma; -a\mathfrak{I}^{-\sigma}) = L^{-1}\left\{\frac{e^{-as^{\sigma}}}{s^{\beta}}\right\},\ \beta > 0,\quad 0 < \sigma < 1$ is the Wright function and.

$\chi_2(\Upsilon, \mathfrak{I}) = \int_0^{\infty} f_2(\Upsilon, u) h(\mathfrak{I}, u) du,$ where $f_2(\Upsilon, \mathfrak{I}) = \frac{1}{2\mathfrak{I}\sqrt{\pi\mathfrak{I}}} \int_0^{\infty} z \exp\left(-\frac{z^2}{4\mathfrak{I}}\right) J_0\left(2\sqrt{a\Upsilon z}\right) dz,$

$h(\mathfrak{I}, u) = h_1(\mathfrak{I}, u) - h_1(\mathfrak{I}, u) * h_2(\mathfrak{I}, u),$ with$h_1(\mathfrak{I}, u) = \delta(t) - \sum_{k=1}^{\infty} \frac{(-bu)^k}{k!} \frac{\mathfrak{I}^{k(\alpha+1)-1}}{\Gamma(k(\alpha+1))},\ h_2(\mathfrak{I}, u) = \sqrt{\frac{u}{\mathfrak{I}}} J_1\left(2\sqrt{u\mathfrak{I}}\right),$.

The function $J_p(\cdot)$ denoted the Bessel functions of the first kind and defined as$J_p(z) = \sum_{m=0}^{\infty} \frac{(-1)^m}{m!\Gamma(m+p+1)} \left(\frac{x}{2}\right)^{2m+p}$..

For the case when $\alpha = 0$, we obtain the classical temperature distribution defined as.

$$T(y, t) = erfc\left(\frac{y\sqrt{\mathrm{Pr}}}{2\sqrt{t}}\right).$$

3.2. Nusselt number

The mathematical expression for the heat transfer rate is given as.

1) For$\alpha \neq 0$.

$$\begin{aligned}Nu &= -\frac{\partial T(\Upsilon, \mathfrak{I})}{\partial \Upsilon}\Big|_{\Upsilon=0} = -\left\{\frac{\partial \bar{T}(\Upsilon, s)}{\partial \Upsilon}\Big|_{\Upsilon=0}\right\} = L^{-1}\left\{\frac{1}{s}\sqrt{\frac{\mathrm{Pr} s^{\alpha+1}}{(1-\alpha)s^{\alpha}+\alpha}}\right\} =\\ &= \sqrt{\frac{\mathrm{Pr}}{1-\alpha}} L^{-1}\left\{\frac{1}{s}\frac{s^{\frac{\alpha+1}{2}}}{\left(s^{\alpha}+\frac{\alpha}{1-\alpha}\right)^{1/2}}\right\} = \sqrt{\frac{\mathrm{Pr}}{1-\alpha}} L^{-1}\left\{\frac{s^{\frac{\alpha-1}{2}}}{\left(s^{\alpha}+\frac{\alpha}{1-\alpha}\right)^{1/2}}\right\}.\end{aligned} \tag{25}$$

We use the Lorenzo-Hartley G-functions,

$$G_{a,b,c}(t, -d) = L^{-1}\left\{\frac{s^b}{(s^a + d)^c}\right\},\ Re(ac - b) > 0$$

In our case$a = \alpha,\ b = \frac{\alpha-1}{2},\ c = 1/2;\ ac - b = 1/2 > 0,$ therefore, the condition is verified.

The inverse Laplace transform Eq. (25) is.

$$Nu = \sqrt{\frac{\mathrm{Pr}}{1-\alpha}} G_{\alpha, \frac{\alpha-1}{2}, \frac{1}{2}}\left(t, -\frac{\alpha}{1-\alpha}\right) \tag{26}$$

2) For $\alpha = 0$, we have.

$$Nu = L^{-1}\left\{\frac{1}{s}\sqrt{\mathrm{Pr} s}\right\} = \sqrt{\mathrm{Pr}} L^{-1}\left\{\frac{1}{\sqrt{s}}\right\} = \sqrt{\frac{\mathrm{Pr}}{\pi t}}.$$

3.3. Velocity field

We get the following results by applying the Laplace transform to Eqs. (8), $(12)_1$, $(13)_1$, and utilizing the initial condition in Eq. $(11)_1$:

$$s\,\bar{\vartheta}(\Upsilon, s) = (1 + \eta s)\frac{\partial^2 \bar{\vartheta}(\Upsilon, s)}{\partial \Upsilon^2} + Gr\,\bar{\chi}(\Upsilon, s), \tag{27}$$

$$\bar{\vartheta}(0, s) = F(s),\ \bar{\vartheta}(\Upsilon, s) \to 0 \text{ as } \Upsilon \to \infty. \tag{28}$$

The solution of Eq. (27) under the conditions of Eq. (28) and using Eq. (22) can be written as.

$$\bar{\vartheta}(\Upsilon,s)=F(s)e^{-\Upsilon\sqrt{\frac{s}{1+\eta s}}}+\frac{Gr}{\left[s-\frac{\Pr(1+\eta s)s^{\alpha+1}}{(1-\alpha)s^{\alpha}+\alpha}\right]}\left[\frac{e^{-\Upsilon\sqrt{\frac{\Pr s^{\alpha+1}}{(1-\alpha)s^{\alpha}+\alpha}}}}{s}-\frac{e^{-\Upsilon\sqrt{\frac{s}{1+\eta s}}}}{s}\right],\tag{29}$$

Eq. (29), can be written as.

$$\bar{\vartheta}(\Upsilon,s)=(sF(s))\bar{\Psi}_1(s)+\bar{\Psi}_2(s)\left[\bar{\chi}(\Upsilon,s)-\bar{\Psi}_1(s)\right],\tag{30}$$

where $\bar{\Psi}_1(s)=\frac{e^{-\Upsilon\sqrt{\frac{s}{1+\eta s}}}}{s}$, $\bar{\Psi}_2(s)=\frac{Gr}{\left[s-\frac{(1+\eta s)s^{\alpha+1}}{(1-\alpha)s^{\alpha}+\alpha}\right]}=Gr\sum_{k=0}^{\infty}\frac{(1-\alpha)\alpha^k s^{-1-\alpha k}+\alpha^{k+1}s^{-1-\alpha-\alpha k}}{\eta^{k+1}\left(s+\frac{\alpha}{\eta}\right)^{k+1}}$.

Applying inverse Laplace transform to Eq. (30) and using the formulas.

$L^{-1}\left\{\frac{e^{-m\sqrt{\frac{as}{s+b}}}}{s}\right\}=1-\frac{2a}{\pi}\int_0^{\infty}\frac{\sin(mz)}{z(a+z^2)}\exp\left(-\frac{bz^2\Im}{a+z^2}\right)dz$ and $G_{\upsilon,\sigma,\tau}(\Im,\lambda)=L^{-1}\left\{\frac{s^{\sigma}}{(s^{\upsilon}-\lambda)^{\tau}}\right\}$, $R(s)>0$, $R(\upsilon\tau-\sigma)>0$, $\left|\frac{\lambda}{s^{\upsilon}}\right|<1$, where $G(\cdot,\cdot)$ being the Lorenzo and Hartley G–function, we obtain.

$$\vartheta(\Upsilon,\Im)=\frac{df(\Im)}{d\Im}*\Psi_1(\Im)+\Psi_2(\Im)*[\chi(\Upsilon,\Im)-\Psi_1(\Im)],\tag{31}$$

where

$$\Psi_1(\Im)=1-\frac{2}{\pi}\int_0^{\infty}\frac{\sin\left(\frac{yz}{\sqrt{\eta}}\right)}{z(1+z^2)}\exp\left(-\frac{z^2\Im}{\eta(1+z^2)}\right)dz,$$

$$\Psi_2(\Im)=Gr\sum_{k=0}^{\infty}\left[\frac{(1-\alpha)\alpha^k}{\eta^{k+1}}G_{1,\,-1-\alpha k,\,k+1}\left(\Im,-\frac{\alpha}{\eta}\right)+\left(\frac{\alpha}{\eta}\right)^{k+1}G_{1,\,-1-\alpha-\alpha k,\,k+1}\left(\Im,-\frac{\alpha}{\eta}\right)\right].$$

For the case when$\alpha=0$, we obtain the classical velocity field defined as.

$$\vartheta(\Upsilon,\Im)=\frac{df(\Im)}{d\Im}*\Psi_1(\Im)+\frac{1}{\eta\Pr}H(t)*\exp\left(\frac{(1-\Pr)t}{\eta\Pr}\right)*\left[erfc\left(\frac{y\sqrt{\Pr}}{2\sqrt{t}}\right)-\Psi_1(\Im)\right],\tag{32}$$

4. Numerical inversion formula

For the validation of our work, we apply the Stehfest's formula [25] for numerical algorithm of inverse Laplace transform method and the compressions are presented in Tables 1 and 2. The Stehfest's formula is defined as.

Table 1 Effect of the volume friction of ternary nanofluid.

ϕ_3	Pr	$\chi(\Upsilon,\Im)$	$q(\Upsilon,\Im)$	$\vartheta(\Upsilon,\Im)$
0	6.03986	0.18196	0.3523	1.02929
0.01	5.96272	0.18564	0.35583	1.04238
0.02	5.88921	0.18921	0.35919	1.05437
0.03	5.81906	0.19269	0.36238	1.06607
0.04	5.75209	0.19606	0.36541	1.0775
0.05	5.68815	0.19933	0.36829	1.08867
0.06	5.62709	0.20251	0.37103	1.09956
0.07	5.56879	0.20559	0.37364	1.11017
0.08	5.51314	0.20857	0.37611	1.12052
0.09	5.46003	0.21145	0.37846	1.13059
0.1	5.40935	0.21424	0.3807	1.14038

Table 2 Effect of the volume friction of hybrid nanofluid.

ϕ_2	Pr	$\chi(\Upsilon,\Im)$	$q(\Upsilon,\Im)$	$\vartheta(\Upsilon,\Im)$
0	6.12879	0.1778	0.34822	1.02929
0.01	6.03986	0.18196	0.3523	1.04275
0.02	5.96042	0.18575	0.35594	1.0551
0.03	5.88466	0.18944	0.35939	1.06718
0.04	5.81228	0.19302	0.36268	1.079
0.05	5.74309	0.19652	0.36581	1.09056
0.06	5.67694	0.19991	0.3688	1.10188
0.07	5.61368	0.20321	0.37163	1.11293
0.08	5.55317	0.20642	0.37433	1.12373
0.09	5.49531	0.20953	0.3769	1.13427
0.1	5.43997	0.21255	0.37935	1.14454

$$\chi_S(\Upsilon,\Im)\cong\frac{\ln(2)}{t}\sum_{j=1}^{2m}d_j\,\bar{\chi}\left(\xi,j\frac{\ln(2)}{t}\right),\tag{33}$$

$$\vartheta_S(\Upsilon,\Im)\cong\frac{\ln(2)}{t}\sum_{j=1}^{2m}d_j\,\bar{\vartheta}\left(r,j\frac{\ln(2)}{t}\right),\tag{34}$$

where$d_j=(-1)^{j+m}\sum_{i=\left[\frac{j+1}{2}\right]}^{\min(j,m)}\frac{i^m(2n)!}{(m-i)!i!(i-1)!(j-i)!(2i-j)!}$, m is a positive integer and $[r]$ denotes the integer value function or bracket function.

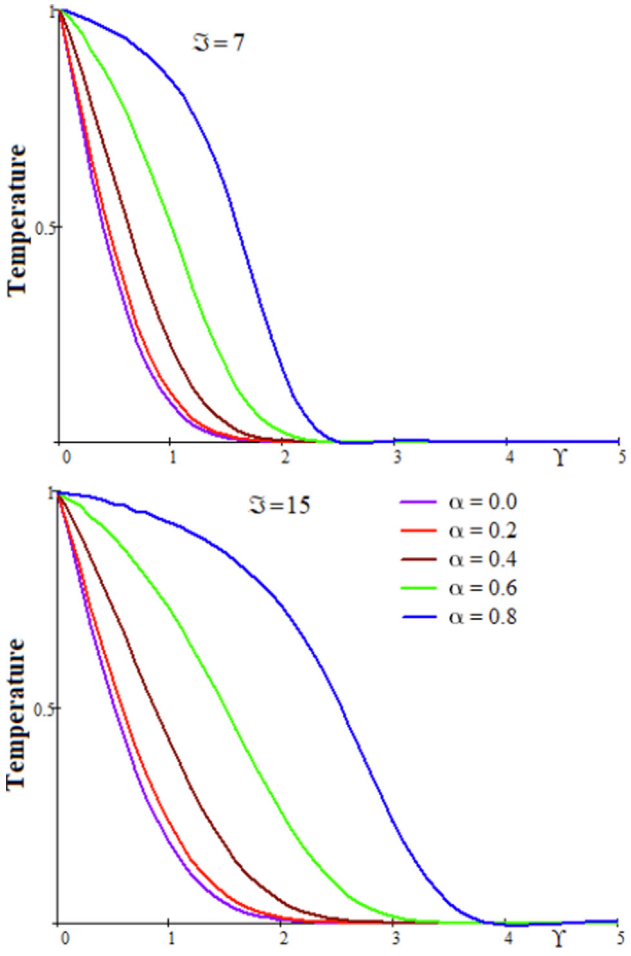

Fig. 1 Profiles of $\chi(\Upsilon,\Im)$ versus Υ for α variation.

5. Numerical results and discussions

The impacts of fractional and physical characteristics on temperature distribution, thermal flux, and velocity field were discussed in this section. With constant heat, we looked at the plate's cosine and sine oscillations. In numerical simulations, we treated Cu, Al_2O_3, and Ag as nanoparticles.

As seen in Eq. (15), the fractional integral is given by a convolution with the power law kernel of fractional parameter. It is clear from this definition that the history of the temperature gradient up to time t, weighted with the convolution kernel, will influence the value of the heat flux from the instant t. The considered model is a mathematical model in which the history of the temperature gradient influences the present thermal process, therefore it is a model with memory. The thermal gradient is damped by the power kernel, therefore the corresponding parameter of the kernel have the role of the memory parameter.

We showed the influence of the fractional parameter α at two different time values in Figs. 1–4. It is observed that when the fractional parameter α is increased, it has an excellent temperature distribution enhancement and the temperature of the system increased. This is due to the fact that as the fractional parameter α is increased, the thermal flux increases. We employed a gemeralized Fourier's law and a temperature distribution that was dependent on the amount of thermal flux. The velocity has a comparable effect, which is to be expected. As time passes, the thermal and boundary layer disparity grows. Due to the definition of fractional integral (see Eq. (15), these influences are provided as the sum of two components. The first portion approaches zero as the fractional parameter approaches 1, whereas the second part has multiple fractional parameters and a singular kernel. Figs. 5 and 6 show the effect of the second-grade fluid parameter. The Newtonian fluid has the most incredible velocity near the plate for short time values, but the influence is opposite for away from the plate. The critical point will vanish for long periods of time. For sine oscillation, the second-grade parameter has a significant impact.

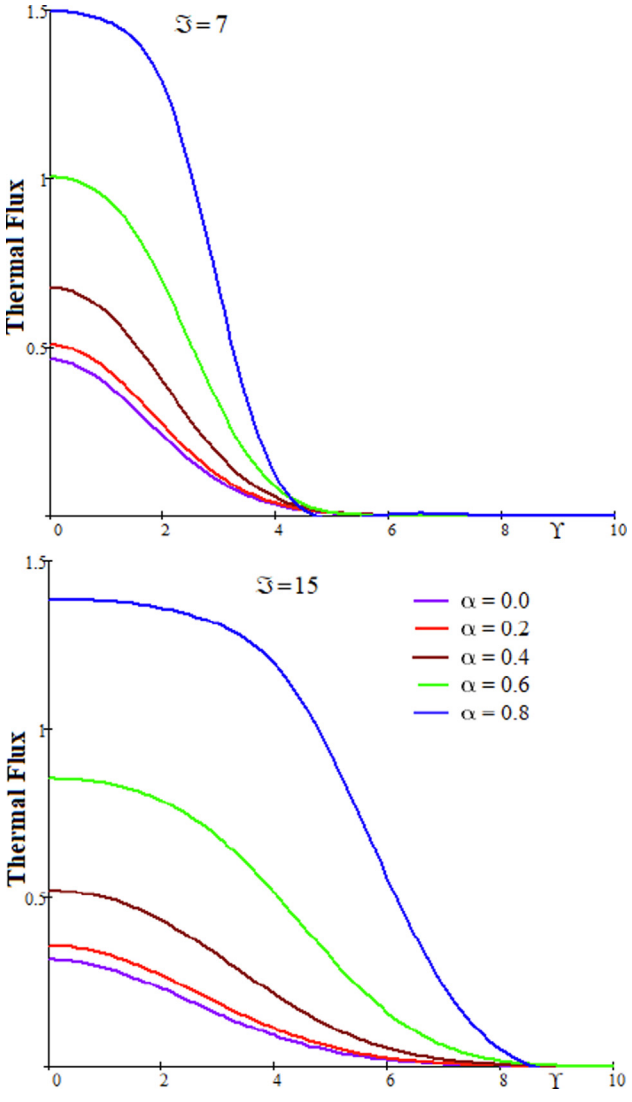

Fig. 2 Profiles of $q(\Upsilon, \Im)$ versus Υ for α variation.

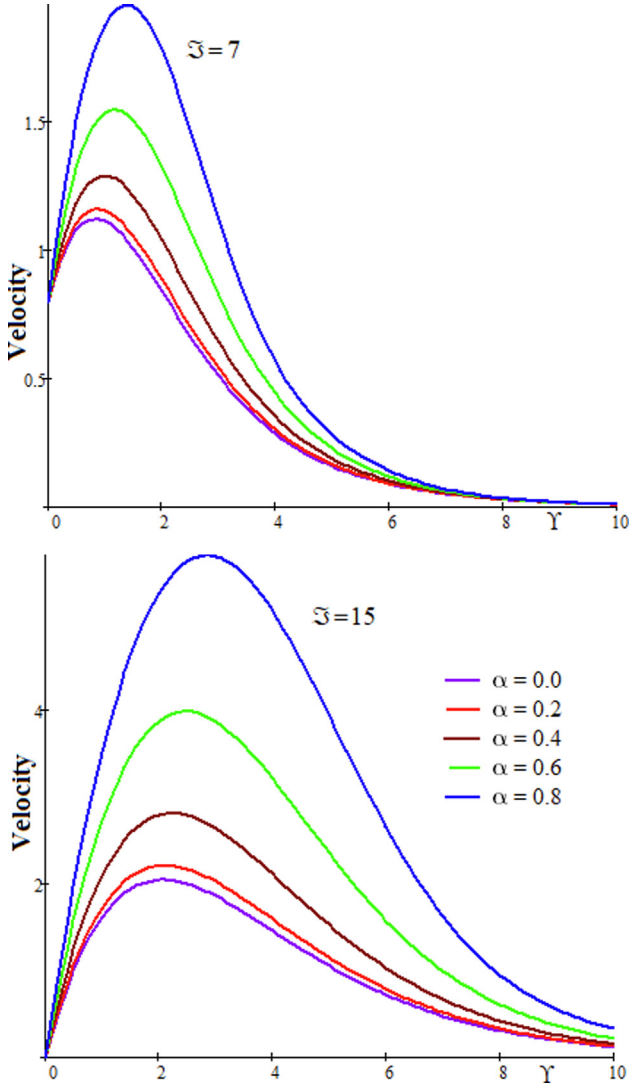

Fig. 3 Profiles of $\vartheta(\Upsilon, \Im)$ versus Υ for α variation with $f(t) = \cos(\pi t/4)$.

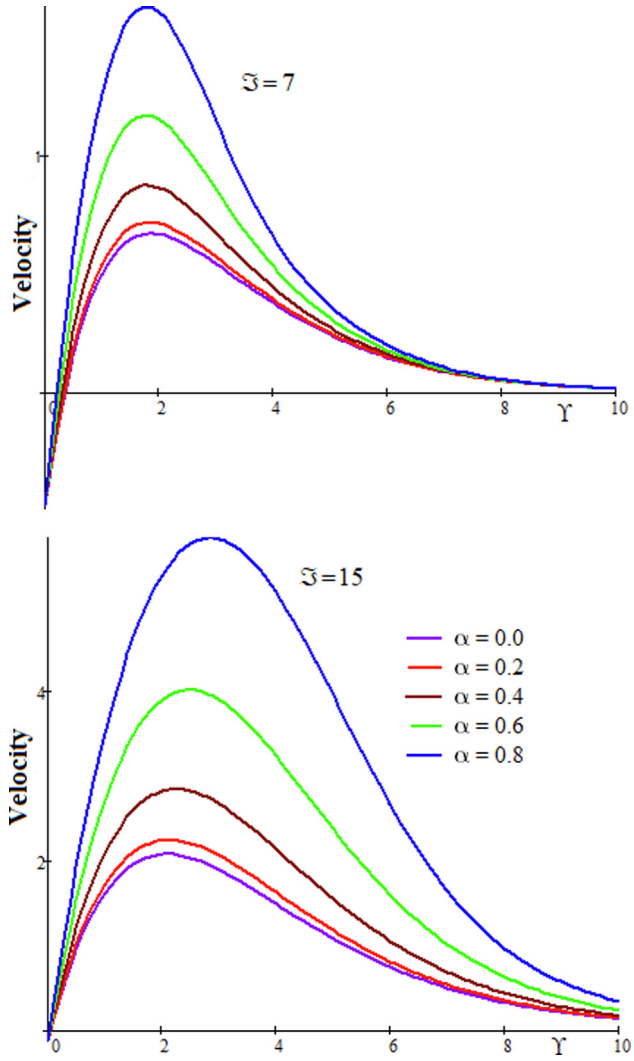

Fig. 4 Profiles of $\vartheta(\Upsilon, \Im)$ versus Υ for α variation with $f(t) = \sin(\pi t/4)$.

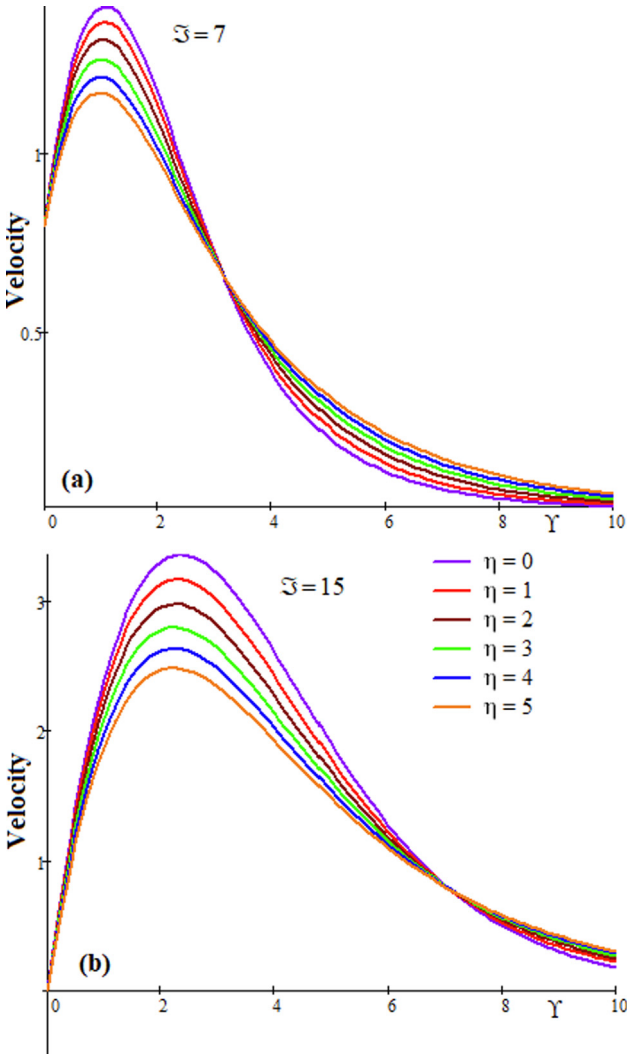

Fig. 5 Profiles of $\vartheta(\Upsilon, \Im)$ versus Υ for η variation with $f(t) = \cos(\pi t/4)$.

Effects of the volume friction of ternary and hybrid nanofluid are presented in Tables 1 and 2. It is observed that by increasing the values of these volume frictions, the Pr number decreases, and the temperature, heat flux, and velocity increase. They are adding the volume friction, which increases the system temperature and velocity.

For the validation of our results, we compare our results with numerical inversion method defined by Stehfest's and presented in Tables 3 And 4. It is observed that the numerical inversion method has a good agreement with our results.

6. Conclusions

In this article, we studied influence of the Atangana-Baleanu (AB) time-fractional integral on second-grade fluid with ternary nanoparticle suspension across an infinite vertical plate. By generalized Fourier's law, the generalized fractional constitutive equation for the thermal flux explains a thermal process with memory. Closed-form solutions are calculated using Laplace transform and represented using Lorenzo and Hartley G–functions and integral forms. The numerical effects of physical and fractional parameters are presented. The observations are:

- By increasing fractional parameter, It has an excellent temperature distribution enhancement.
- The velocity has a comparable effect, which is to be expected. As time passes, the thermal and boundary layer disparity grows.
- The Newtonian fluid has the most incredible velocity near the plate for short time values, but the influence is opposite for away from the plate. The critical point will vanish for long periods of time.
- For sine oscillation, the second-grade parameter has a significant impact.
- By increasing the values of these volume frictions, the Pr number decreases, and the temperature, heat flux, and velocity increase.
- The numerical inversion method has a good agreement with our results.

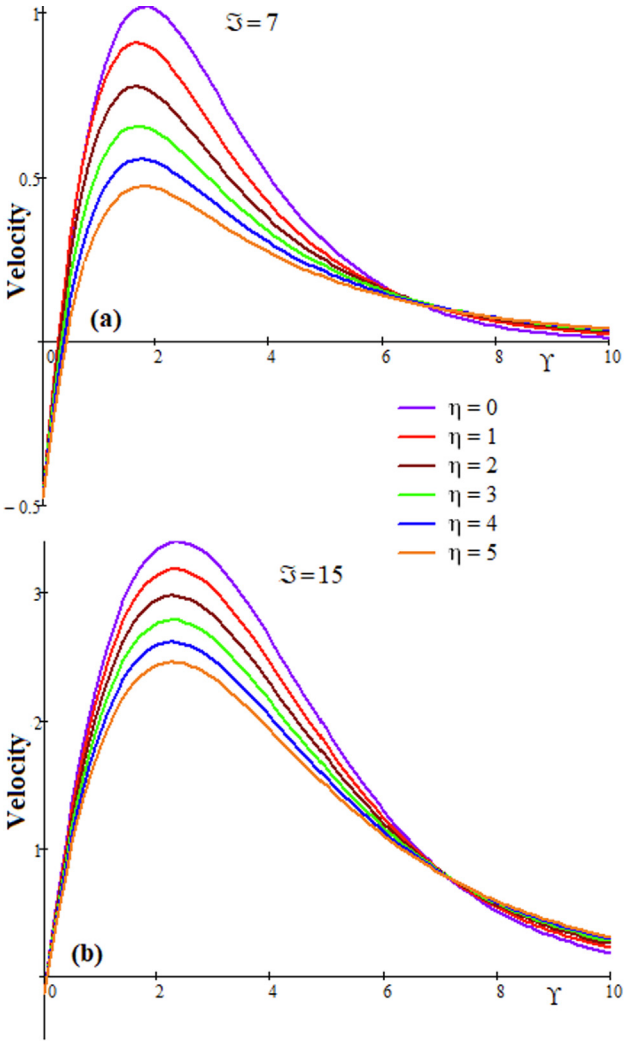

Fig. 6 Profiles of $\vartheta(\Upsilon,\Im)$ versus Υ for α variation with $f(t) = \sin(\pi t/4)$.

Table 3 Comparison of temperature distribution with inversion method y.

y	$\chi(\Upsilon,\Im)$; Eq. (24)	$\chi_S(\Upsilon,\Im)$; Eq. (33)	$\lvert\chi(\Upsilon,\Im) - \chi_S(\Upsilon,\Im)\rvert$
0	1	1	0
0.1	0.98274322	0.98455667	0.00181345
0.2	0.96091618	0.9677866	0.00687042
0.3	0.95290404	0.94958017	0.00332387
0.4	0.93405618	0.92981783	0.00423835
0.5	0.90807069	0.90836443	0.00029374
0.6	0.88242409	0.88508683	0.00266273
0.7	0.85826375	0.85987906	0.00161531
0.8	0.83311703	0.83267174	0.0004453
0.9	0.80489138	0.8034225	0.00146888
1	0.77319345	0.77209892	0.00109453

Declaration of Competing Interest

The authors declare that they have no known competing financial interests or personal relationships that could have appeared to influence the work reported in this paper.

Table 4 Comparison of velocity field with inversion method.

y	$\vartheta(\Upsilon,\Im)$; Eq. (24)	$\vartheta_S(\Upsilon,\Im)$; Eq. (33)	$\lvert\vartheta(\Upsilon,\Im) - \vartheta_S(\Upsilon,\Im)\rvert$
0	0.70711	0.79204	0.08494
0.1	0.83412	0.92565	0.09153
0.2	0.94784	1.04444	0.0966
0.3	1.04864	1.14894	0.10031
0.4	1.13689	1.23973	0.10284
0.5	1.21301	1.31735	0.10434
0.6	1.27745	1.38236	0.10491
0.7	1.33071	1.43536	0.10465
0.8	1.37328	1.47693	0.10365
0.9	1.40567	1.50769	0.10202
1	1.42843	1.52827	0.09984

Acknowledgement

This work was conducted under the Technology Innovation Program (or Industrial Strategic Technology Development Program-material part package type) as "Development of fire suppression-type high safety module and demonstration of safety for future eco-friendly medium and large secondary battery (No. 20015986)", funded by the Ministry of Trade, Industry & Energy (MOTIE), Republic of Korea.

References

[1] A.M. Alsharif, Y. Abd Elmaboud, Electroosmotic flow of generalized fractional second grade fluid with fractional Cattaneo model through a vertical annulus, Chin. J. Phys. (2021), https://doi.org/10.1016/j.cjph.2021.08.021.

[2] A.I. Abdellateef, H.M. Alshehri, Y.A. Elmaboud, Electro-osmoticflow of fractional second-grade fluid with fractional Cattaneo heat flux through a verticalmicrochannel, Heat Transfer. 50 (7) (2021) 6628–6644, https://doi.org/10.1002/htj.22195.

[3] M. Caputo, F. Mainardi, A new dissipation model based on memory mechanism, Pure Appl. Geophys. 91 (1971) 134e147.

[4] M. Caputo, F. Mainardi, Linear model of dissipation in anelastic solids, Rivis tael Novo Cimento 1 (1971) 161e198.

[5] M. Caputo, Vibrations on an infinite viscoelastic layer with a dissipative memory, J. Acoust. Soc. Am. 56 (1974) 897e904.

[6] M.A. Ezzat, Thermoelectric MHD with modified Fourier's law, Int. J. Therm. Sci. 50 (4) (2011) 449–455.

[7] M.A. Ezzat, Thermoelectric MHD non-Newtonian fluid with fractional derivative heat transfer, Physica B 405 (2010) 4188–4194.

[8] E. Bas, R. Ozarslan, Real world applications of fractional models by Atangana-Baleanu fractional derivative, Chaos Solitons Fractals 116 (2018) 121–125, https://doi.org/10.1016/j.chaos.2018.09.019.

[9] M. Saqib, A.R. Mohd Kasim, N.F. Mohammad, D.L. Chuan Ching, S. Shafie, Application of fractional derivative without singular and local kernel to enhanced heat transfer in CNTs nanofluid over an inclined plate, Symmetry (Basel) 2020, 12, https://doi.org/10.3390/SYM12050768.

[10] D. Kumar, J. Singh, K. Tanwar, D. Baleanu, A new fractional exothermic reactions model having constant heat source in porous media with power, exponential and Mittag-Leffler laws, Int. J. Heat Mass Transf. 138 (2019) 1222–1227, https://doi.org/10.1016/j.ijheatmasstransfer.2019.04.094.

[11] M.A. Ezzat, A.S. El-Karamany, A.A. El-Bary, M.A. Fayik, Fractional calculus in one-dimensional isotropic thermo-viscoelasticity, C. R. Mecanique 341 (2013) 553–566.

[12] N.A. Shah, J.D. Chung, D. Vieru, C. Fetecau, Unsteady flows of Maxwell fluids with shear rate memory and pressure-dependent viscosity in a rectangular channel, Chaos Solitons Fractals 148 (2021) 111078.
[13] Y.A. Elmaboud, Two-layered electroosmotic flow through a vertical microchannel with fractional Cattaneo heat flux, J. Taibah Univ. Sci. 15 (2021) 1, https://doi.org/10.1080/16583655.2021.2016162.
[14] M.A. Ezzat, M.Z. Abd-Elaal, State space approach to viscoelastic fluid flow of hydromagnetic fluctuating boundary-layer through a porous medium, ZAMM. Z. angew. Math. Mech. 77 (3) (1997) 197–207.
[15] M.A. Ezzat, M.Z. Abd-Elaal, Free convection effects on a viscoelastic boundary layer flow with one relaxation time through a porous medium, J. Franklin Institut. 334 (4) (1997) 685–706.
[16] N. Ahmed, D. Vieru, C. Fetecau, N.A. Shah, Convective flows of generalized time-nonlocal nanofluids through a vertical rectangular channel, Phys Fluids 30 (5) (2018) 052002, https://doi.org/10.1063/1.5032165.
[17] M. Tanveer, S. Ullah, N.A. Shah, Thermal analysis of free convection flows of viscous carbon nanotubes nanofluids with generalized thermal transport: a Prabhakar fractional model, J. Therm. Anal. Calorim. 144 (6) (2021) 2327–2336.
[18] Y.-X. Li, M.I. Khan, R.J.P. Gowda, A. Ali, S. Farooq, Y.-M. Chu, S.U. Khan, Dynamics of aluminum oxide and copper hybrid nanofluid in nonlinear mixed Marangoni convective flow with entropy generation: Applications to renewable energy, Chinese J. Phys. 73 (2021) 275–287, https://doi.org/10.1016/j.cjph.2021.06.004.
[19] N. Ahmed, N.A. Shah, D. Vieru, Natural convection with damped thermal flux in a vertical circular cylinder, Chinese J. Phys. 56 (2) (2018) 630–644.
[20] T. Elnaqeeb, N.A. Shah, A. Rauf, Natural convection flows of carbon nanotube Prabhakar-like fractional second-grade nanofluids over an infinite plate with Newtonian heating, Math. Methods Appl. Sci. (2020), https://doi.org/10.1002/MMA.6795.
[21] Z.U. Nisa, N.A. Shah, I. Tlili, S. Ullah, M. Nazar, Natural convection flow of second grade fluid with thermal radiation and damped thermal flux between vertical channels, Alexandria Eng. J. 58 (4) (2019) 1119–1125.
[22] L. Syam Sundar, S. Mesfin, Y. Tefera Sintie, V. Punnaiah, A.J. Chamkha, A.C.M. Sousa, A Review on the use of hybrid nanofluid in a solar flat plate and parabolic trough collectors and its enhanced collector thermal efficiency, J. Nanofluids 10 (2) (2021) 147–171.
[23] Y. Mahsud, N.A. Shah, D. Vieru, Natural convection flows and heat transfer with exponential memory of a Maxwell fluid with damped shear stress, Comput. Math. Appl. 76 (9) (2018) 2246–2261.
[24] N.A. Shah, C. Fetecau, D. Vieru, Natural convection flows of Prabhakar-like fractional Maxwell fluids with generalized thermal transport, J. Therm. Anal. Calorim. 143 (3) (2021) 2245–2258.
[25] H. Stehfest, Algorithm 368: numerical inversion of Laplace transforms, Commun. ACM 13 (1970) 47–49.